

# From Nanorods to Atomically Thin Wires of Anatase TiO<sub>2</sub>: Nonhydrolytic Synthesis and Characterization

Chenmin Liu, Hui Sun, and Shihe Yang\*<sup>[a]</sup>

**Abstract:** A nonhydrolytic two-step chemical process has been developed to synthesize ultrathin, nearly monodisperse TiO<sub>2</sub> (anatase) wires with tunable diameters of 5 nm to approximately 4 Å, reaching the atomic length scale. The high-quality anatase titania atomically thin wires can be doped and stabilized with nitrogen species by introducing suitable nitrogen-containing mole-

cules. The ultrathin wires, particularly the atomically thin wires, as well as the precursor, have been thoroughly characterized by an extensive series of structural, spectroscopic, and other

**Keywords:** nanostructures • size effects • synthetic methods • thin wires • titanium dioxide

techniques. Possible formation mechanisms for the rods and the wires are proposed on the basis of experimental results obtained under varying reaction conditions. Also demonstrated are the pronounced effects of size and N-doping on the electronic, optical, and phononic properties of the anatase titania wires in the smallest size regime.


## Introduction

Synthetic chemistry has been the workhorse for bottom-up fabrication of nanomaterials.<sup>[1–3]</sup> In principle it offers atomic precision and bonding specificity with added advantages of controllability, processibility, cost-effectiveness, and scalability. The ability to synthesize size-tunable quantum dots that has been developed in the last two decades represents a grand triumph of the bottom-up chemical approach,<sup>[4–8]</sup> but generalization of this methodology to the controllable synthesis of nanostructures of different materials with different sizes and shapes is still a major challenge. In particular, control over nanowire growth is often rather limited in terms of the nanowire quality and size. It is especially difficult to obtain ultrathin nanowires of uniform size. Although some ultrathin nanowires have been recently reported,<sup>[9–11]</sup> it is still unclear how they can be synthesized, stabilized, and manipulated in general terms. Ultimately, the controllable synthesis of atomically thin wires would be of interest. The

quantum effect is most pronounced in this size regime reaching the atomic limit, and the change in size and shape is often accompanied by a dramatic change in electronic structure and thus in physical and chemical properties. Control over size- and shape-dependent electronic structures should allow adjustment of the intrinsic properties of any material; this principle has been practiced for meeting the demands of a wide range of applications.

Widely known as white pigments in the form of anatase and rutile, titanium dioxide (TiO<sub>2</sub>) is also intensively studied and extensively used in heterogeneous catalysis, photocatalysis (water purification, air cleaning, water splitting for the production of hydrogen and electricity), solar cells, gas sensors, corrosion-protective coatings, ceramics, dielectric and optical materials, Li-ion battery electrodes, and electric devices such as varistors.<sup>[12–18]</sup> The functionality of many of the titania-based devices can be boosted and significantly amplified by virtue of two aspects of atomic engineering: size reduction to nanoscale and atomic doping. The former leads to pronounced confinement and surface effects, whereas the latter introduces local chemical and electronic effects, both of which contribute to the modification and augmentation of material properties. For example, underlying the optical response of a given material is normally its electronic structure, which can be tuned by reducing its physical dimensions to the nanometer regime (confinement of carriers) and by varying its chemical composition. In its pure form, titania has limited UV-driven activity, which largely inhibits its overall efficiency under natural sunlight (5% UV, 300–

[a] Dr. C. Liu, H. Sun, Prof. Dr. S. Yang  
Department of Chemistry  
William Mong Institute of Nano Science and Technology  
The Hong Kong University of Science and Technology  
Clear Water Bay, Kowloon (Hong Kong)  
Fax: (+852) 2358-1594  
E-mail: chsyang@ust.hk

 Supporting information (MALDI-TOF mass spectra, HPLC profiles, and <sup>13</sup>C NMR spectra) for this article is available on the WWW under <http://dx.doi.org/10.1002/chem.200902524>.

400 nm; 43 % visible, 400–700 nm; and 52 % IR, 700–2500 nm).<sup>[19]</sup> One of the potential solutions for improving its efficiency is to shift its absorption from the UV into the visible region, allowing more photons to be absorbed and utilized. By changing the chemical composition of TiO<sub>2</sub> through main-group doping, in particular with nitrogen, it has been shown that the resultant nitrogen-doped TiO<sub>2</sub> is capable of light activity at much longer wavelengths.<sup>[20–23]</sup> Thus, TiO<sub>2</sub> doped with nitrogen (N-TiO<sub>2</sub>) has received a great deal of attention in the past few years owing to its potential role in solving the currently exacerbating global energy and environmental crises.<sup>[24–30]</sup> Depending on the specific application, the TiO<sub>2</sub> as well as the N-TiO<sub>2</sub> materials must fulfill a wide variety of requirements in terms of particle size, size distribution, morphology, crystallinity, and phase. Up to now, many TiO<sub>2</sub> and N-TiO<sub>2</sub> nanostructures, for example, nanofilms, hollow spheres, nanotubes, nanowires, and mesoporous structures, have been synthesized by different methods including hydrolytic, sol–gel, electrophoretic, and thermal deposition.<sup>[12,17,18,31–41]</sup> However, there is still only limited control over the growth of the nanostructures obtained from solution chemical synthesis.

Recently we gave a preliminary report on the synthesis of extremely thin wires of N-doped anatase titania reaching the Å regime.<sup>[42]</sup> This opens opportunities not only to explore the physical properties and application of the atomically thin wires but also to understand their growth and doping processes. Herein, we present a comprehensive study on the synthesis and characterization of atomically thin titania wires (4–5 Å) and of ultrathin titania nanorods (<5 nm). Our synthesis is based on a simple nonhydrolytic two-step approach, which consists of controlled precursor formation involving ester elimination, esterification, and controlled precursor condensation involving the oxidation of amines with ester elimination. Furthermore, we demonstrate a facile method of N-doping and its attendant stabilization of the titania atomically thin wires. Finally, we demonstrate the pronounced effects of size and N-doping on electronic, optical, and phononic properties of the anatase titania wires traversing the nm to Å scales.

## Results and Discussion

**Size and morphology of titania wires:** The products collected after precursor treatment at different temperatures for different reaction time periods were examined by using transmission electron microscopy (TEM, see Figure 1). As expected, the precursor obtained from the first solvothermal step is an amorphous gel network without any crystalline material (Figure 1A). However, after the second heat treatment at 180 °C for 1 h in the presence of octadecene (ODE), well-dispersed atomically thin wires with a mean diameter of approximately 4.5 Å and mean length of approximately 20 nm were achieved (Figure 1B). When the same solvothermally prepared precursor was post-treated at 180 °C for 12 h, we obtained long and bundled atomically thin wires (average diameter 0.5 nm, average length ≈38 nm; Figure 1C). However, when the heat treatment was at 300 °C for 20 min, well-dispersed nanorods with a mean diameter of approximately 3 nm and length of approximately 11 nm were obtained (Figure 1D), and prolonging the post-treatment process to 1 h resulted in nearly monodisperse nanorods with the same mean diameter (≈3 nm) but the mean length increased to approximately 19 nm (Figure 1E). When the second heating process was further prolonged to 3 h, we obtained a self-assembled pattern of bundled nanorods, a typical example of which is shown in Figure 1F. It thus appears that a longer heat treatment time

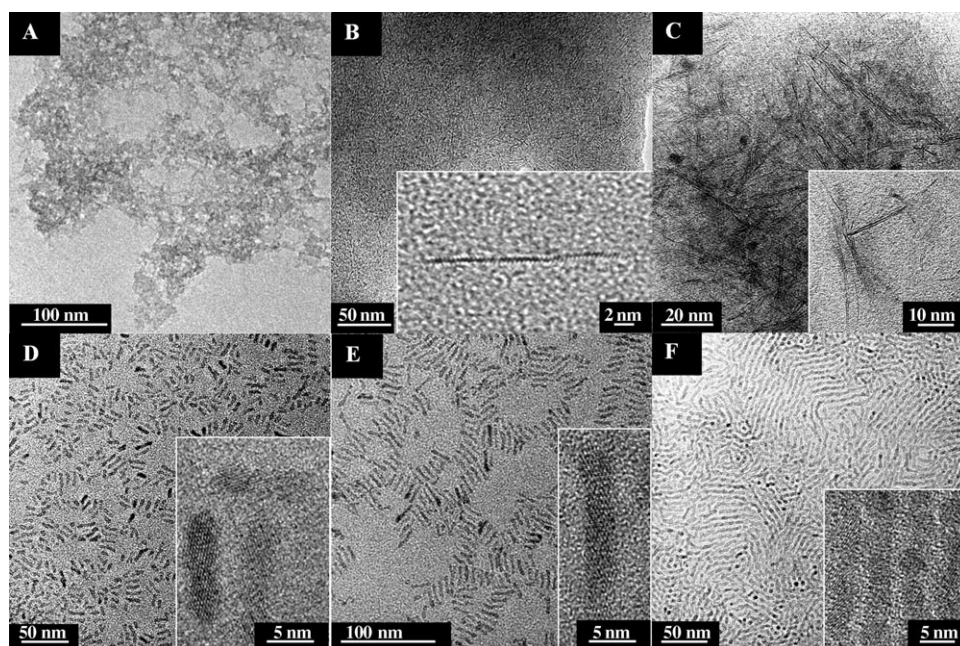


Figure 1. TEM micrographs showing the evolution of products from the Ti complex precursor to atomically thin anatase titania wires and nanorods and their self-assembled networks: A) the titanium complex precursor obtained in the first step of solvothermal treatment; B) dispersed atomically thin wires obtained after precursor treatment in ODE for 1 h at 180 °C; C) bundled atomically thin TiO<sub>2</sub> wires obtained after precursor treatment in ODE for 12 h at 180 °C; D) TiO<sub>2</sub> nanorods obtained after precursor treatment in ODE for 20 min at 300 °C; E) TiO<sub>2</sub> nanorods obtained after precursor treatment in ODE for 1 h at 300 °C; F) TiO<sub>2</sub> nanorod network obtained after precursor treatment in ODE for 3 h at 300 °C. Insets of B–E: Enlarged HRTEM images of the corresponding nanostructures.

tends to increase the lengths but not the diameters and favors bundling and self-assembly of both the nanorods and the atomically thin wires.

We found that the sequence in which oleylamine (OLA) was added to the reaction mixture can have important effects on the bundling and self-assembly of the wires, and to illustrate this point we conducted a one-pot solvothermal synthesis. When OLA was added before the start of the reaction at 150°C for 25 h, closely assembled, ultrathin titania nanowires ( $\approx 1.8$  nm) were obtained (Figure 2 A). However,

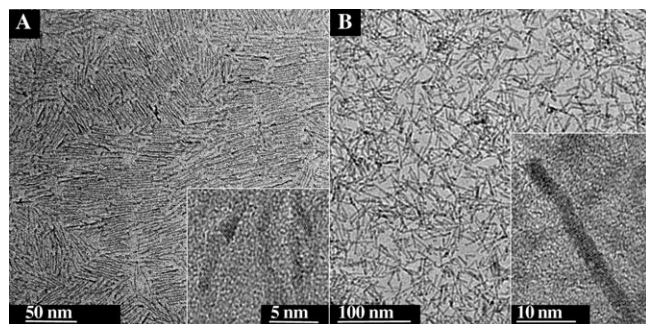


Figure 2. A)  $\text{TiO}_2$  nanowires ( $d \approx 1.8$  nm) obtained in a one-step synthesis in which OLA was pre-added to the reaction mixture; B)  $\text{TiO}_2$  nanorods ( $d \approx 3.0$  nm) obtained by hot injection of OLA. Insets: Enlarged HRTEM images of the corresponding nanowires.

hot injection, whereby OLA was added dropwise during the reaction with the same reagents, gave well-separated titania nanowires (Figure 2B). These results suggest that a pre-formed uniform mixture of oleic acid (OA) and OLA solution favors self-assembly of the wires, which is perhaps due to the tendency to form an ordered micelle structure.<sup>[11,43,44]</sup>

As described above, by careful tuning of the reaction conditions the smallest-diameter, atomically thin titania wires could be obtained in both isolated and bundled forms depending on the reaction time. More detailed TEM and high-resolution TEM (HRTEM) characterizations were carried out on the spatially separated, atomically thin wires. The atomically thin wires were abundant with lengths of up to 20 nm and diameters that were uniformly below 6 Å, and typically around 4–5 Å (Figure 3 A). The good dispersion of the atomically thin wires, free of aggregation and bundling, on the copper grid can be attributed to the protective surface layer of OA. A survey of several atomically thin wires in higher-magnification TEM images (an example is shown in Figure 3 B) further confirms that the diameters of these wires are indeed in the 4–5 Å range, with an average of 4.5 Å. Note that the atomically thin wires are crystalline with well-defined lattice fringes spaced at about 0.35 nm (Figure 3B),

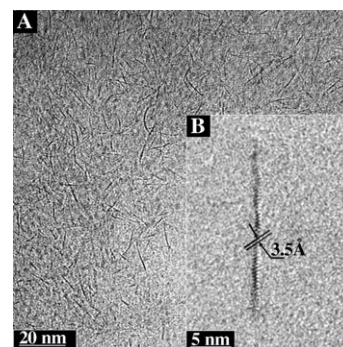


Figure 3. TEM micrographs of atomically thin N- $\text{TiO}_2$  wires grown at 180°C for 1 h: A) an overview image of nearly monodispersed, atomically thin wires; B) HRTEM image of a single atomically thin wire ( $d \approx 4.5$  Å). The individual atomically thin wire is crystalline with lattice fringes spaced at approximately 3.5 Å, corresponding to the spacing between the (101) planes of anatase  $\text{TiO}_2$ .

which corresponds to the spacing between the (101) planes of anatase  $\text{TiO}_2$ .

Table 1, which summarizes the synthesis results we have obtained so far from a series of experiments, clearly shows the effects of the reaction conditions on the size and morphology of the titania wires. This is also schematically illustrated in Figure 4. Whereas an increase in reaction temperature mainly increased the wire diameter, prolongation of the precursor treatment time mainly caused an increase in the wire length accompanied by bundling and self-assembly, which was promoted by OLA. This can provide a valuable guide for controlling the 1D structures of titania. Note that the atomically thin wires, nanowires, and nanorods of titania exhibit good shelf stability in ambient conditions. For example, the atomically thin titania wires could still maintain their diameters and morphologies after storage for more than a year.

**Composition and bonding structures:** The composition of the products was ascertained and checked by X-ray photoelectron spectroscopy (XPS). The estimated atomic concentrations from typical XPS survey spectra of the precursor, atomically thin wires, nanorods ( $1.8 \times 38$  nm,  $3 \times 19$  nm), and commercial P25 nanoparticles (diameter  $\approx 20$  nm; Figure 5 A) over a broad binding-energy range are given in Table 2. For the atomically thin wires with an O/Ti atomic

Table 1. Size and shape of the products obtained under various precursor treatment conditions.<sup>[a]</sup>

Temp [°C]	Duration [h]	Morphology	Mean diam [nm]	Mean length [nm]
180	1	separated atomically thin wires (> 90 %)	$0.5 \pm 0.1$	$20.0 \pm 3.8$
180	12	bundled atomically thin wires (> 80 %); nanodots (< 20 %)	$0.5 \pm 0.2$	$38.2 \pm 5.3$
300	1/3	nanorods	$3.1 \pm 0.2$	$11.7 \pm 3.3$
300	1	nanorods	$3.0 \pm 0.2$	$18.6 \pm 2.3$
300	3	nanorod network pattern	$3.0 \pm 0.2$	–
150 (one-pot solvothermal)	25	nanowires	$1.8 \pm 0.1$	$38.0 \pm 1.9$

[a] The parameters were estimated from the TEM data.

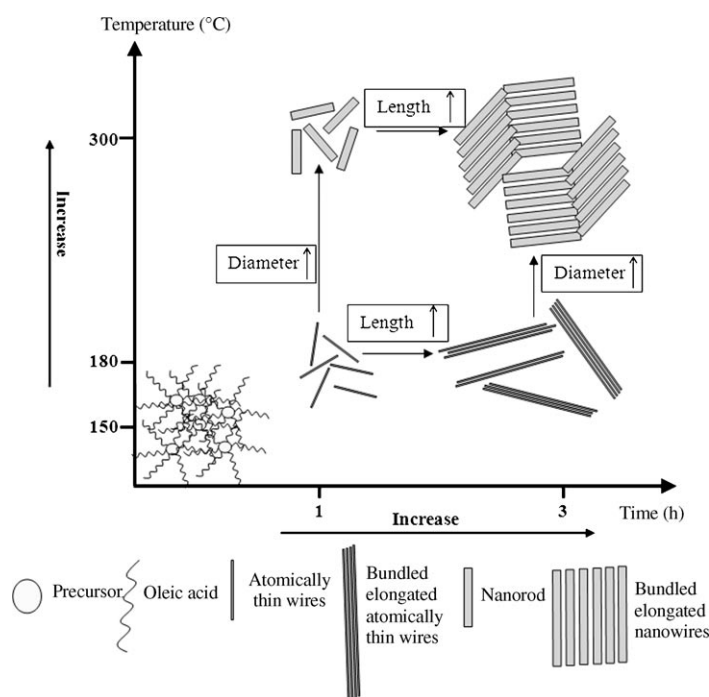


Figure 4. Schematic representation of the evolution of the product morphology as a function of reaction temperature and time.

ratio of approximately 3.6:1, the extra oxygen atoms can be ascribed to the contribution from the capping layer of OA. As a result, with the increase in size (precursor  $\rightarrow$  atomically thin wires  $\rightarrow$  ultrathin nanowires  $\rightarrow$  nanorods  $\rightarrow$  relatively large nanoparticles) and thus a decrease in the surface/volume ratio, the O content decreases. This is because, ultimately, the bulk titania has an O/Ti ratio of only 2:1. To our surprise, the N/Ti atomic ratio is as high as 0.24:1, which is far beyond the environmental contamination level ( $\approx 0.01:1$  in the P25 sample, see Table 2) and hence indicates N-doping in the atomically thin anatase wires. Interestingly, we found that both OLA and  $N_2$ , introduced separately into the reaction system in the second heat-treatment step, could effectively dope the atomically thin wires with nitrogen.

For further analysis of the chemical structure of the intermediate, product, and reference samples, three areas of the XPS spectra, namely the N1s around 400 eV, the Ti2p near 460 eV, and the O1s around 530 eV, were examined more closely. The relatively high intensity of the N1s peak for the atomically thin wires (Figure 5B) again proves the existence of N-doping, contrary to the remaining samples. Furthermore, the N1s peak of the atomically thin N-TiO<sub>2</sub> wires is centered at approximately 401 eV. We have previously shown that the N1s peak is not from the free OLA ( $\approx 399$  eV) used as a reagent in the synthesis.<sup>[42]</sup> We also suggest here that the N1s peak is not from the OLA simply coordinated to Ti atoms of the atomically thin wires, which would result in a binding energy of approximately 400 eV.<sup>[45]</sup> The N1s peak at approximately 401 eV is notably higher than that in TiN crystals with a typical N1s binding energy of approximately 397 eV. Because the core-electron binding

energy of an atom is usually higher when the oxidation state of the atom is more positive, the N1s peak with a relatively high binding energy can be ascribed to nitrogen species in a relatively high oxidation state, such as in NC or NCO, or to an NO site in titania.<sup>[46–49]</sup> This can be explained by the fact that the N1s electron binding energy is 408 eV in NaNO<sub>3</sub> but 398 eV in NH<sub>3</sub>.<sup>[45]</sup> When the nitrogen atoms in TiN are partially replaced or oxidized by O atoms to form such a structure as O–Ti–N or O–Ti–O–N on the atomically thin wire surfaces, the electron density around N will be reduced owing to the strong electron-withdrawing ability of the O atoms, leading to an increased N1s binding energy.<sup>[25,29,49]</sup> The above argument has excluded the possibility of direct OLA coordination to the surface Ti atoms, so the relatively high N1s binding energy we observed suggests that the N-doping of the atomically thin TiO<sub>2</sub> wires may well take the structural form O–Ti–O–N–C on the atomically thin wire surfaces. More discussion on this aspect will be found below.

In addition, the facile N-doping in the atomically thin titania wires is in marked contrast to the little N-doping in the titania nanowires. This could be attributed to the larger surface-to-volume ratio and higher surface activity of the atomically thin wires than of the nanowires. In our experience the N-doping not only modifies the electronic structure of the materials but also appears to have the effect of stabilizing the atomically thin titania wires further. Specifically, we found that the atomically thin wires of pure titania were unstable under electron-beam irradiation and hence it is much more difficult to obtain clear TEM images, but the atomically thin N-TiO<sub>2</sub> wires were much more stable in this sense. This is why the TEM images presented above are almost all for the atomically thin N-TiO<sub>2</sub> wires. Such a stabilization effect is believed to result from the nitrogen dopant passivation on the part of the wire surface not adequately covered by OA.

From the O1s XPS spectra of the four titania samples together with fitting results obtained by using XPSPEAK Version 4.1 software (Figure 5C and D), one can see significant changes upon precursor decomposition and atomically thin wire growth in comparison with the reference P25 nanoparticles. Figure 5D<sup>[1–4]</sup> shows the fitted O1s spectra for the precursor, atomically thin wires, and nanorods, respectively. The signal at a relatively high binding energy of approximately 532 eV in the O1s spectrum was previously assigned to surface-anchored, oxygen-containing species, such as  $-\text{COO}-$ ,  $-\text{C}-\text{N}-\text{O}-$  or  $-\text{OH}$ ,<sup>[45]</sup> which in our case is denoted as “Peak I” (Figure 5D). The lower binding-energy peak can be ascribed to oxygen atoms that are bound to atoms of lower electronegativity such as in  $\text{Ti}-\text{O}-\text{Ti}$ ,<sup>[45]</sup> which we have denoted as “Peak II” (Figure 5D). These assignments are consistent with the much greater abundance of the ligand oxygen (a large Peak I) than of the Ti-connected lattice oxygen (a small Peak II) in the precursor. On the other hand, no apparent Peak I can be observed for P25 nanoparticles (see Figure 5C) because of their much larger size, and hence much smaller relative surface area. Indeed, in the order nanorod  $\rightarrow$  ultrathin nanowires  $\rightarrow$  atomically thin

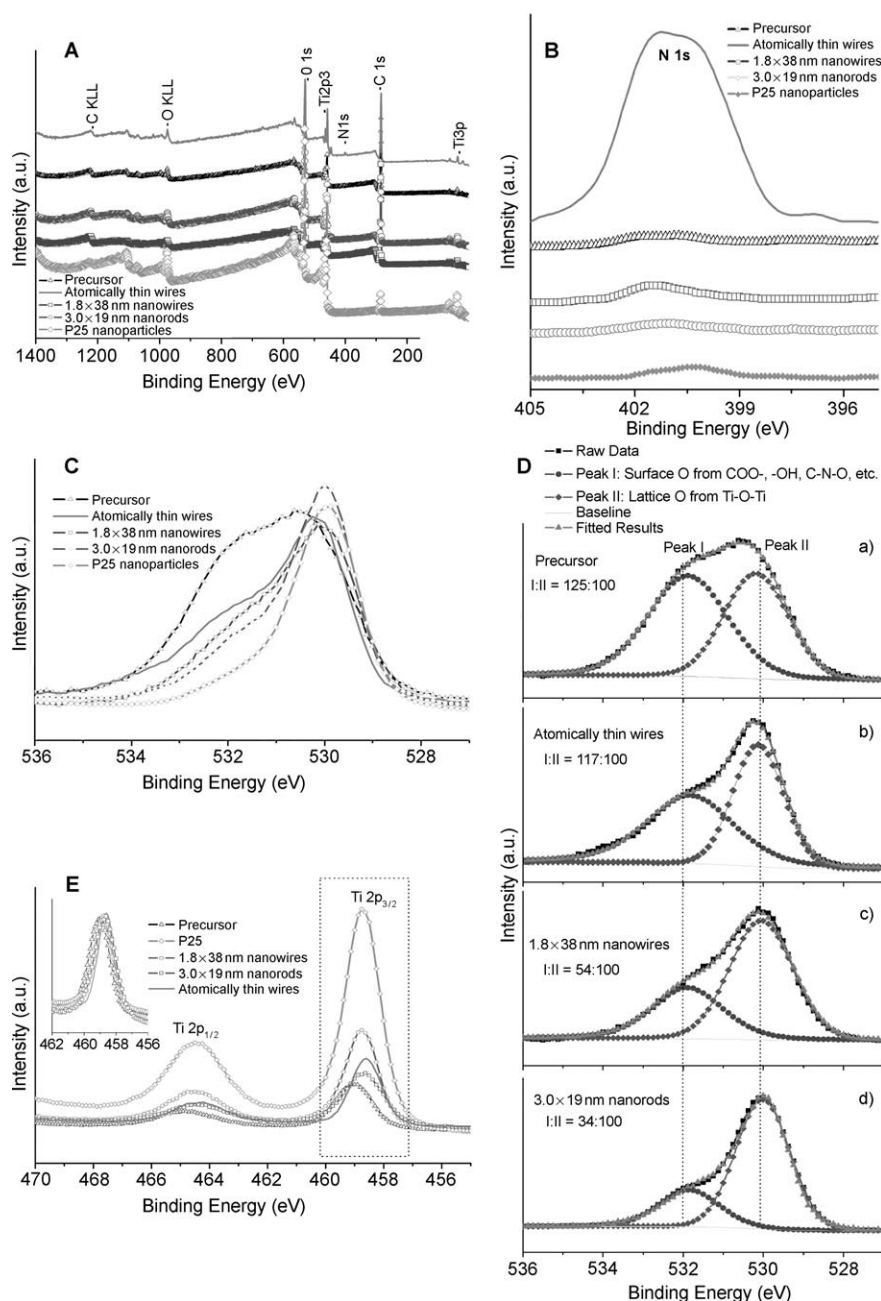


Figure 5. A) XPS survey spectra of precursor, atomically thin N-TiO<sub>2</sub> wires, 1.8 × 38 nm nanowires, 3 × 19 nm nanorods, and P25 nanoparticles; B) XPS spectra in the N 1s region around 400 eV; C) XPS spectra in the O 1s region at around 530 eV; D) fitted O 1s spectra for precursor a), atomically thin wires b), 1.8 × 38 nm nanowires c), and 3 × 19 nm nanorods d); E) XPS spectra in the Ti 2p region at around 460 eV (inset: a magnified portion of Ti 2p<sub>3/2</sub> at around 459 eV).

Table 2. Relative atomic contents of the products calculated from XPS data.

Sample	Ti 2p	O 1s	N 1s
Precursor	1	3.60	0.03
Atomically thin wires	1	3.27	0.24
1.8 × 38 nm nanowires	1	3.16	0.08
3 × 19 nm nanorods	1	2.70	0.02
P25	1	2.33	0.01

wires → precursor, with decreasing size the ratio of ligand oxygen (Peak I) to Ti-connected lattice oxygen (Peak II) dramatically increases as can be seen from Figure 5D 1–4, owing to the dramatically increasing surface/volume ratio. This trend reflects the change in O contributions to the O 1s spectra from the carboxylic groups in precursors and atomically thin wires, in comparison with those from the anatase TiO<sub>2</sub> lattice in nanorods and P25 nanoparticles. Also noteworthy are the shifts of the peaks. As can be seen in Figure 5D, the O 1s peak associated with the Ti–O–Ti lattice at approximately 530.2 eV (Figure 5D 1, Peak II) for the precursor is slightly shifted to approximately 530.1 eV (Figure 5D 2, Peak II) for atomically thin wires, to approximately 530.0 eV (Figure 5D 3, Peak II) for nanowires with diameters of 1.8 nm, and to 529.9 eV (Figure 5D 4, Peak II) for nanorods with diameters of 3.0 nm and for P25 nanoparticles (Figure 5C), whereas no obvious shift could be observed in the surface ligand O 1s peak (Figure 5D 1–4, Peak I) for the series of samples. There are two possible causes of this phenomenon: the size reduction and the surface effect, both of which are likely to increase the electron binding energy. The size reduction is due to electron confinement, whereas the surface effect is a consequence of the high electronegativity of the ligand.

The Ti 2p spectra (Figure 5E) confirm that the oxidation state of titanium in all four samples

is mainly +4, considering that the signals centered at around 458.7 eV (Ti 2p<sub>3/2</sub>) and 464.3 eV (Ti 2p<sub>1/2</sub>) are similar to those of fully oxidized bulk TiO<sub>2</sub>. However, by scanning the Ti 2p region in detail, subtle differences for the four samples also become noticeable. There is a signal for the precursor at around 459.1 eV, which is a notably higher binding energy than those for the remaining samples (Figure 5E, inset). This phenomenon is also caused by the spe-

cial structure of R-COO-Ti-OOC-R. Specifically, because of the high electron-withdrawing ability of the surrounding R-COO- group, the electron density around the Ti atom is reduced; this results in the increase in Ti binding energy. Also note that the Ti2p<sub>3/2</sub> peak at 458.6 eV for the nitrated atomically thin wires is smaller by approximately 0.3 eV than that for the commercial P25 TiO<sub>2</sub> nanoparticles. Two explanations are possible for the N-induced Ti2p binding-energy shift: 1) the P25 nanoparticles may have a more highly strained Ti<sup>4+</sup> environment, and the incorporation of the nitrogen species may relieve the strain;<sup>[25,26]</sup> 2) the substitution of nitrogen for oxygen could enhance the electron density at Ti<sup>4+</sup> or partially change the valence state of Ti<sup>4+</sup> to Ti<sup>3+</sup>, which would also lower the binding energy of the Ti2p<sub>3/2</sub> peak.<sup>[50]</sup>

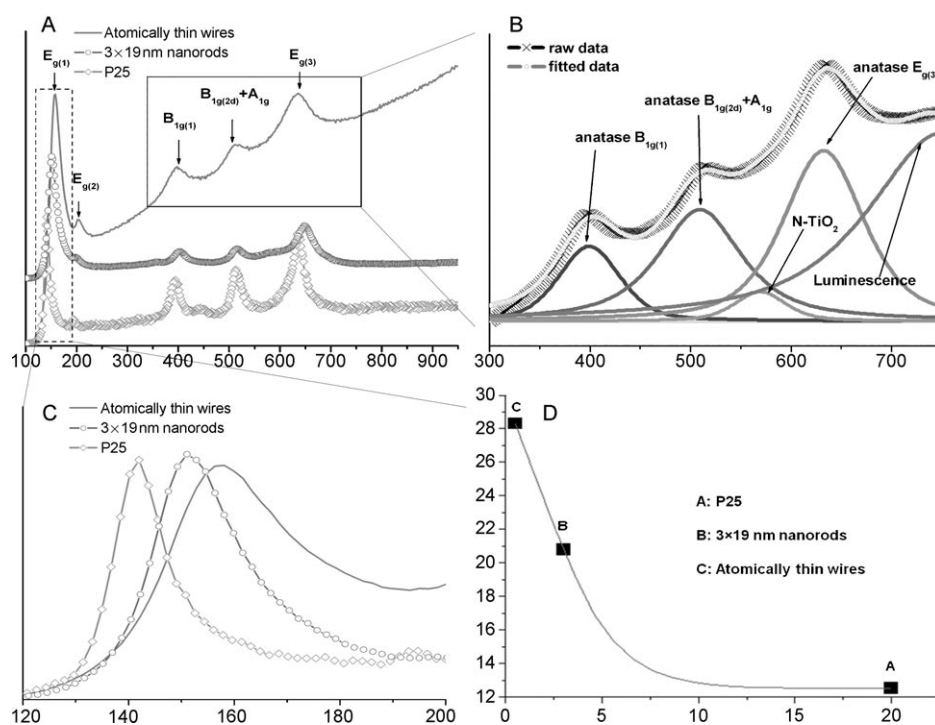


Figure 6. Raman spectra of the titania products excited at 514 nm: A) overall Raman spectra of the atomically thin N-TiO<sub>2</sub> wires, 3 × 19 nm nanorods, and P25 nanoparticles; B) an enlarged Raman spectrum of the atomically thin N-TiO<sub>2</sub> wires in the solid-line rectangle in A) together with the fitted result; C) an enlarged Raman spectra of the dashed-line rectangle in A), indicating the shift of the E<sub>g(1)</sub> Raman signal with the size of the nanostructures; D) FWHMs of the E<sub>g(1)</sub> Raman signal for different samples plotted versus the size of the nanostructures. The solid line is a guide for the eye.

## Raman scattering and phonon

**confinement:** The bulk anatase TiO<sub>2</sub> has six Raman-active fundamentals in the vibrational spectrum: three E<sub>g</sub> modes centered around 142, 196, and 639 cm<sup>-1</sup> (designated here as E<sub>g(1)</sub>, E<sub>g(2)</sub>, and E<sub>g(3)</sub>, respectively), two B<sub>1g</sub> modes at 399 and 519 cm<sup>-1</sup> (designated B<sub>1g(1)</sub> and B<sub>1g(2d)</sub>, respectively), and an A<sub>1g</sub> mode at 513 cm<sup>-1</sup>. In these vibrational modes, E<sub>g(3)</sub>, B<sub>1g(2d)</sub>, and A<sub>1g</sub> are of the Ti-O bond-stretching type, whereas the modes of B<sub>1g(1)</sub>, E<sub>g(1)</sub>, and E<sub>g(2)</sub> are associated with the O-Ti-O bending vibrations.<sup>[51]</sup> As the crystallite size decreases, each of the Raman signals shows increased broadening and systematic frequency shifts; the latter can be blueshifts and redshifts for different Raman signals.<sup>[52]</sup> Such Raman signal broadening and frequency shifting trends have all been confirmed in the Raman spectra of our atomically thin wires and nanorods, as shown in Figure 6 and in Table 3. For example, with the decrease in crystallite size, the most intense Raman signal of E<sub>g(1)</sub> at around 142 cm<sup>-1</sup> is broadened by as much as nearly 20 cm<sup>-1</sup> (see Figure 6D). Such signal broadening also occurred for other Raman signals, although to a smaller extent (see Figure 6A). As for signal positions, the E<sub>g(1)</sub> mode showed the largest blueshift with decreasing crystal size (see Figure 6C and Table 3): 142 cm<sup>-1</sup> for nanoparticles with diameters of approximately 25 nm, 151 cm<sup>-1</sup> for 3 × 19 nm nanorods, and 158 cm<sup>-1</sup> for atomically thin wires. A smaller blueshift was seen for the E<sub>g(2)</sub> mode: 206 cm<sup>-1</sup> for atomically thin wires, 199 cm<sup>-1</sup> for

Table 3. Raman signal positions [cm<sup>-1</sup>] in different titania samples.

Sample	E <sub>g(1)</sub>	E <sub>g(2)</sub>	B <sub>1g(1)</sub>	B <sub>1g(2d)</sub> + A <sub>1g</sub>	E <sub>g(3)</sub>
Atomically thin wires	158.0	205.9	401.3	508.7	635.3
3 × 19 nm nanorods	151.0	199.2	401.6	514.6	648.6
P25	141.6	194.0	394.9	514.0	636.7

nanorods, and 196 cm<sup>-1</sup> for P25 nanoparticles. The B<sub>1g(1)</sub> mode showed an even smaller blueshift: approximately 400 cm<sup>-1</sup> for atomically thin wires and nanorods, and 396 cm<sup>-1</sup> for P25 nanoparticles. For the combined B<sub>1g(2d)</sub>+A<sub>1g</sub> modes, redshifts were observed instead: 508 cm<sup>-1</sup> for atomically thin wires and 514 cm<sup>-1</sup> for P25 nanoparticles. For the anatase material, the most intense E<sub>g(1)</sub> mode is commonly chosen for phonon analysis owing to its characteristic features, such as the largest broadening and the largest blueshift as described above. To appreciate the trends better, we compared the E<sub>g(1)</sub> signal positions for the samples of different sizes in Figure 6C and plotted the full-width at half maximum (FWHM) of this signal as a function of size in Figure 6D. The dramatic blueshifts and signal broadening are clearly seen as the wire diameter is decreased in this size range, a range that probably exhibits the most dramatic size effects.

The availability of the atomically thin anatase wires allowed us to acquire the Raman data in the smallest size

region, which give rise to the most pronounced Raman signal broadening and shifts. In the literature, the size effect on the Raman scattering in nanocrystalline  $\text{TiO}_2$  is commonly interpreted as originating from phonon confinement.<sup>[13,53–57]</sup> Although the phonon-confinement model is thought to be inapplicable for nanocrystals smaller than 3 nm,<sup>[58,59]</sup> the Raman signal broadening and shifts follow surprisingly consistent and clear trends. We believe that in our case some other factors, such as nonstoichiometry<sup>[60,61]</sup> of titanium and oxygen, or internal stress/surface tension effects<sup>[62]</sup> arising from the drastic dimensional reduction to atomic-scale wires, may also play an important role in the broadening and shift of the Raman signal, but the detailed explanations call for further experimental as well as theoretical studies.

The presence of a strong luminescence background (see Figure 6B), which must be included in the fitting of the Raman spectrum, should be mentioned. Such visible-light-induced luminescence from the atomically thin  $\text{TiO}_2$  wires is a direct manifestation of the N-doping effect previously observed in other forms of the anatase  $\text{TiO}_2$ .<sup>[26]</sup> This will be discussed further below.

**Optical spectroscopy and electronic structure:** Figure 7A shows UV/Vis absorption spectra of N- $\text{TiO}_2$  atomically thin wires and  $3 \times 19$  nm titania nanorods. First, in the UV region (below 300 nm), an absorption signal at approximately 269 nm was observed for the nanorods, whereas this signal is blueshifted by approximately 12 nm to approximately 257 nm for the atomically thin wires. This blueshift is presumably due to the reduction in the wire diameter as documented in earlier reports.<sup>[63,64]</sup> The absorption of the titania nanorods was limited only to the UV region, whereas the absorption threshold value of atomically thin N- $\text{TiO}_2$  wires was extended from 270 to 600 nm. This is consistent with the fact that the atomically thin wires are dark yellow, whereas the nanorods appear to be very pale yellow, nearly

white, which demonstrates a pronounced effect of the surface doping of nitrogen species on the optical response of the atomically thin wires in the visible-wavelength region. Such an absorption edge shift was generally observed in  $\text{TiO}_2$  materials with bulk doping of nitrogen species,<sup>[13,23,26,65]</sup> and was attributed to additional N-dopant-induced energy bands. Livraghi et al. found that N- $\text{TiO}_2$  contained single-atom nitrogen impurity centers, localized in the bandgap of the oxide, which were responsible for visible-light absorption by promoting electrons from the localized gap states to the conduction band.<sup>[30]</sup> Serpone proposed that the commonality in all doped titanias rests with formation of oxygen vacancies and color centers; the latter were thought to account for the redshift of the absorption edge.<sup>[66]</sup> However, because almost all the atoms of our atomically thin  $\text{TiO}_2$  wires are on the surface, the doping of N species is probably on the surface and involves oxidative coupling of OLA.

In the photoluminescence (PL) spectra of the anatase wires with different diameters (Figure 7B and C), the first observation is a dramatic blueshift of approximately 68 nm to around 303 nm for the bandgap emission of the atomically thin wires compared with large P25 anatase nanocrystals, and to the much smaller blueshifts for the 1.8 nm ( $< 10$  nm) and the 3.0 nm ( $< 5$  nm)  $\text{TiO}_2$  nanorods. This is consistent with the fact that the typical exciton Bohr radius of anatase  $\text{TiO}_2$  is 1.5 nm. In other words, when the diameter of an anatase nanowire is approaching and/or smaller than the exciton Bohr radius, the bandgap emission is expected to display a prominent blueshift.<sup>[64]</sup> Second, as shown in Figure 7C, another signal observed at approximately 590 nm in the visible region for the atomically thin wires is mainly due to the intergap states arising from the surface N-doping.<sup>[12,13,23,26,67–69]</sup> However, for the sample synthesized by the one-pot solvothermal method (1.8 nm nanowires), the visible signal is at a much longer wavelength ( $\approx 720$  nm); it is believed to be associated with transitions of electrons from the conduction band edge to holes, trapped at interstitial  $\text{Ti}^{3+}$  sites arising

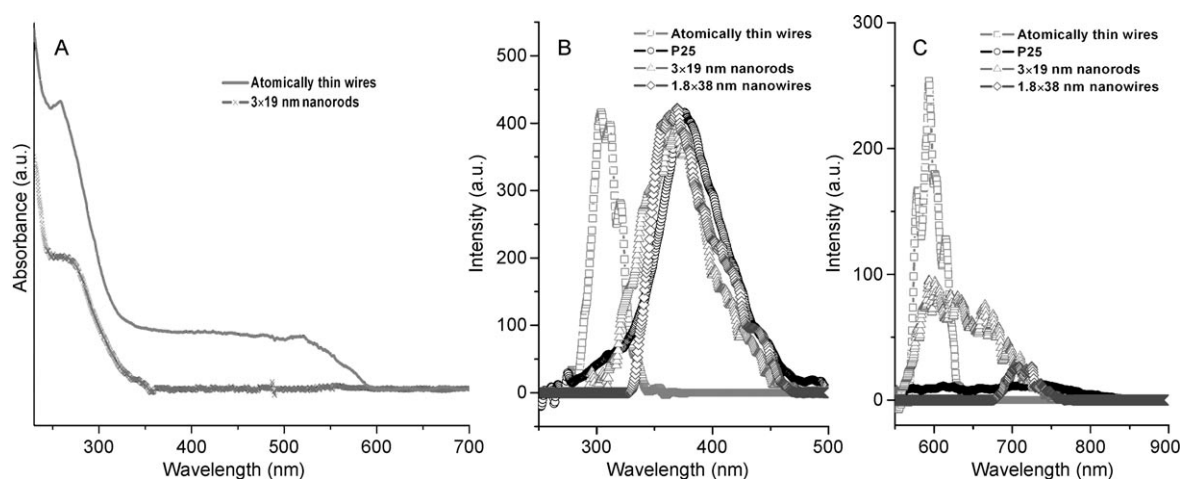


Figure 7. Spectra of A) UV/Vis absorption spectra of atomically thin N- $\text{TiO}_2$  wires and  $3 \times 19$  nm nanorods; B) UV photoluminescence spectra of atomically thin N- $\text{TiO}_2$  wires,  $1.8 \times 38$  nm nanowires,  $3 \times 19$  nm nanorods, and P25 nanoparticles; C) visible photoluminescence spectra of atomically thin N- $\text{TiO}_2$  wires,  $3 \times 19$  nm nanorods, and P25 nanoparticles. The excitation for B) and C) was at 270 nm.

from surface defects of the nanorods.<sup>[63,64]</sup> For the 3 nm nanorods, a much broader signal in the region of 550–750 nm was observed, which appears to consist of both types of PL described above. Finally, a weak but broad signal in the region of 550–800 nm can be recognized for the commercial P25 sample. This signal was previously attributed to the interfacial  $\text{Ti}^{4+}\text{--OH}$  (500–650 nm)<sup>[70]</sup> and interstitial  $\text{Ti}^{3+}$  sites (650–800 nm).<sup>[63,64]</sup> These results clearly show that the surface N-doping of the atomically thin wires results in distinct enhancements not only in visible absorption but also in visible luminescence. As mentioned above, nitriding of  $\text{TiO}_2$  nanoparticles is expected to create localized impurities and/or defects and give rise to additional energy bands,<sup>[13,20]</sup> which, besides supporting the visible-light absorption, could also boost visible-light luminescence.<sup>[12,13,20,23,26]</sup>

**Electron spin resonance and photoinduced carrier generation:** To investigate possible involvement of localized impurities and defects in the visible absorption and PL of atomically thin N- $\text{TiO}_2$  wires, ESR spectroscopy was performed on these samples. Figure 8A highlights changes in the ESR spectrum of atomically thin N- $\text{TiO}_2$  wires under white-light illumination generated by a 150 W halogen light source compared with the ESR spectrum taken in the dark. The most important observation is a pronounced enhancement of the ESR signals upon light irradiation, which clearly points to carrier generation in the atomically thin N- $\text{TiO}_2$  wires after light absorption. Remarkably, this occurs even at room temperature, at which light-induced ESR signal enhancement could rarely be observed for other  $\text{TiO}_2$  materials. Moreover, the light-induced ESR signals could persist for over 6 h after the light was turned off, indicating persistent trapping with only a very slow decay of the photogenerated carriers. The light-induced ESR signals, although also present in the dark, were sharp and shifted somewhat compared with those in the dark. Presumably, the photogenerated carriers were trapped at different sites with different lifetimes and most of them would eventually decay by recombination, leaving the most deeply trapped carriers, which appear to be similar to those in the dark.

It is well documented for titania materials that ESR signals with  $g$  values of less than 2.0 are due to trapped electrons associated with  $\text{Ti}^{3+}$  centers, whereas those in the 2.00–2.03 range correspond to trapped holes.<sup>[71–77]</sup> The spectroscopic splitting factor  $g$  can be obtained from Equation (a), in which  $\nu$  is the frequency of the electromagnetic radiation (9.40 G in our experiment),  $\mu_B$  is the Bohr magneton, and  $H_0$  (mT) is the magnetic field strength.

$$g = h\nu/\mu_B H_0 \quad (\text{a})$$

After substitution of the constants, Equation (a) can be simplified to  $g = 21.42 \times 9.40/(3.00 \times 10^8 \times H_0)$ . The resulting  $g$  values are given in Figure 8 for atomically thin N- $\text{TiO}_2$  wires. We tentatively assign the ESR signals at  $g = 2.013$  to trapped holes, and those at  $g = 1.999$  and 1.994 to trapped electrons.<sup>[71–77]</sup> In other words, the photogenerated electrons are mainly trapped at two types of sites, and there is only one main trapping site for the photogenerated holes.<sup>[30,49,77]</sup> In addition, the ESR signal of the photogenerated holes is much weaker, probably owing to recombination with surface electron donors.

With the above information in mind, we can interpret the ESR result in terms of surface traps of our atomically thin, OA-capped N- $\text{TiO}_2$  wires. The singular feature of the atomically thin wires is that almost all of the atoms are on the wire surfaces. The surface titanium atoms, in general, experience a very different crystal-field environment (for example, a distorted octahedral crystal field) from that of the bulk atoms. This creates abundant electron-trapping centers with different values of  $g$  factors.<sup>[77]</sup> Two types of electron-trapping sites can be envisaged in our atomically thin N- $\text{TiO}_2$  wires: one from N coordination, and the other from the OA capping. The former is believed to correspond to the weak ESR signal at  $g = 1.999$  and the latter to the strongest ESR signal at  $g = 1.994$ . The ESR signal at  $g = 2.013$  can be ascribed to holes localized on the N centers.<sup>[30,49,71–77]</sup> Moreover, the energy levels of both electron- and hole-trapping centers are located in the bandgap of  $\text{TiO}_2$ , which accounts for the visible-light sensitivity of the atomically thin N- $\text{TiO}_2$

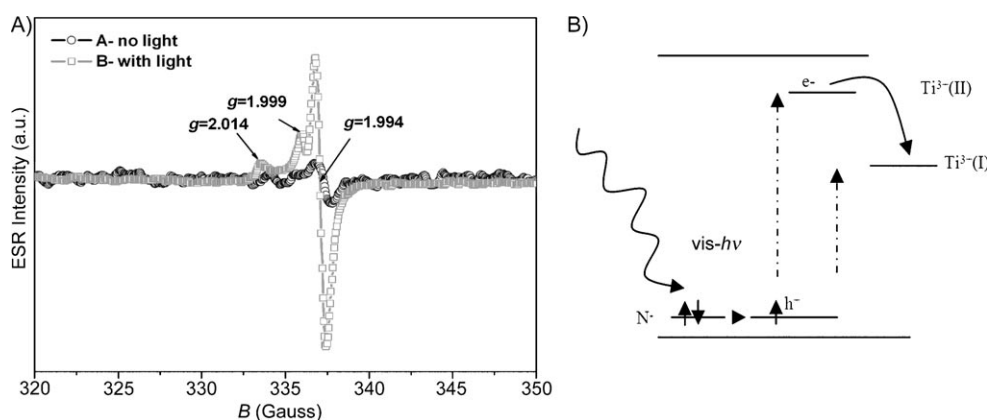
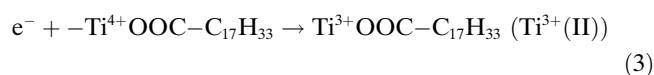
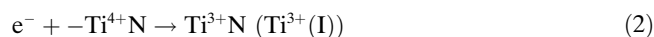


Figure 8. A) ESR spectra of N- $\text{TiO}_2$  atomically thin wires in the dark and under white-light illumination at room temperature; B) schematic energy levels illustrating the proposed mechanism for the visible-light induced carrier processes in N- $\text{TiO}_2$  atomically thin wires.

wires. Reactions (1)–(3) make up a sequence of visible-light-induced events that are probably involved in the formation of trapped electrons and holes in atomically thin N-doped TiO<sub>2</sub> wires.



A picture then emerges for the photoinduced ESR signals from our atomically thin N-TiO<sub>2</sub> wires; the photoinduced carrier generation process outlined above is schematically illustrated in Figure 8B. Upon illumination with visible light, electrons are released from the N centers and trapped on the surfaces (with either N or OA coordination corresponding to Ti<sup>3+</sup>(I) and Ti<sup>3+</sup>(II), respectively, as shown in Figure 8B), leaving behind the holes on the N centers, which could also be replenished by electrons from surface donors.

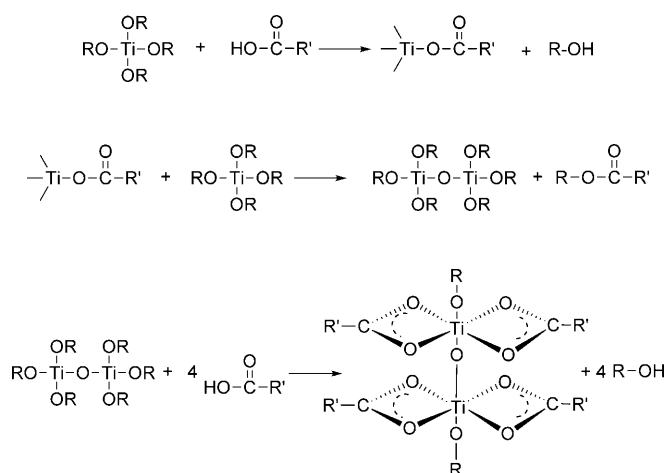
As a reference, when the same ESR measurements were performed on the titania nanorods at room temperature, no obvious signal could be detected. This indicates that either the density of photogenerated electrons and holes is negligible or the lifetimes of the photogenerated electrons and holes are too short to be observed in the ESR spectra. Both possibilities may exist. The former is due to the much lower visible absorption of the nanorods than of the atomically thin wires, and the latter may be related to the enhanced carrier trapping of the photogenerated carriers.

#### Mechanistic implications for the growth of the ultrathin nanowires:

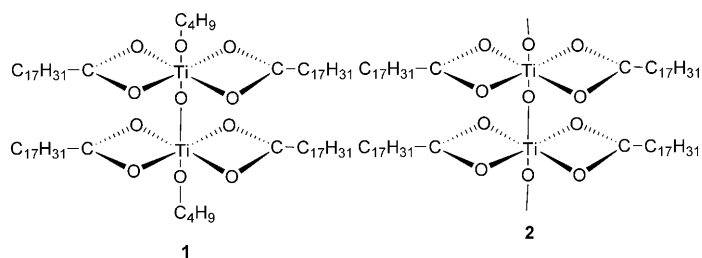
Some immediate questions about the atomically thin TiO<sub>2</sub> wires warrant attention, for example, how were they formed? In our experiments, we found that they could also be formed under appropriate conditions without the solvothermal precursor-preparation step, but the yield was relatively low. Then why did the two-step process increase the atomically thin-wire yield? What is the nature of the N-doping process? First, it is commonly found that aqueous hydrolysis of titanium alkoxide or titanium chloride precursors results in the formation of spherical TiO<sub>2</sub> nanoparticles, whereas nonhydrolytic decomposition of titanium oleate precursors yields anisotropic TiO<sub>2</sub> nanostructures. This means that a slow reaction (for example, a nonhydrolytic process) would favor 1D growth of TiO<sub>2</sub>. With a further stretch of the imagination, thinner and thinner TiO<sub>2</sub> nanowires, and ultimately atomically thin wires, could be formed under milder and milder conditions. This seems to be what we have observed here. Specifically, our results show that a relatively low reaction temperature, together with appropriate amounts of oxygen and humidity, is conducive to the formation of atomically thin TiO<sub>2</sub> wires. This is clearly demonstrated in Figures 1–4 and Table 1. We also found that the diameters of the products are more closely related to the reaction temperature, whereas their lengths are more closely

related to the reaction time (see Figure 4). When the reaction temperature was 180 °C, well-separated atomically thin wires could be obtained, but when it was raised to approximately 300 °C, the diameter of the products dramatically increased to over 2 nm. This increase in diameter may be caused by the increased aminolysis rate at the elevated temperature, which is sufficient to turn on the mode of sideways growth. By balancing the reaction temperature and reaction time, diameter-tunable, ultrathin titania nanowires could be obtained. Next, the benefit of a two-step process appears to lie in the separation of the processes of precursor formation and atomically thin wire growth so as to optimize both and prevent mutual interference of the two. Finally, the characterization data obtained so far indicate that the N-doping originates from the oxidative coupling of OLA to surfaces of the atomically thin wires, forming the N–O–Ti surface structure. We believe that the N-doping stabilizes the atomically thin TiO<sub>2</sub> wire structure because the N species, as a type of cosurfactant, can passivate part of the atomically thin wire surface that somehow has not been capped adequately or completely by OA in the absence of the N species. Indeed, high-quality TEM images could be easily obtained for atomically thin N-TiO<sub>2</sub> wires, but not for those without N doping.

The subsequent questions are then: What actually is the precursor? How is it formed and how is it transformed ultimately into the titania wires? We believe that in the first step of precursor formation, the titanium butoxide is esterified nonhydrolytically and dimerized by ester elimination,<sup>[31,35]</sup> as expressed by Reactions (4)–(6) taking place in the autoclave.

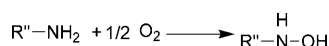


MALDI-TOF mass spectrometry (see the Supporting Information) provided molecular information about the precursor. In separate measurements on precursor samples prepared separately at different times, a mass signal consistently appeared at *m/z* values of 1270–1280 (Figures S1A and B) in the Supporting Information). The mass signals correspond very closely to **2** at *m/z* ≈ 1268, which is presumably a



fragment of the precursor **1** ( $R = C_4H_9$ ,  $R' = C_{17}H_{33}$ ) after elimination of the butyl groups. This MS result supports the precursor-forming Reactions (4)–(6).

We next consider the second step: the precursor formed in the first step,  $(C_{17}H_{33}COO)_2(OC_4H_9)_2Ti-O-Ti(OC_4H_9)(OOC-C_{17}H_{33})_2$ , is polycondensed to form ultrathin titania wires. When the reaction was at  $180^\circ C$  in ambient conditions, the polycondensation rate was slow, a condition necessary for generating atomically thin wires. Here the trace amount of water in ambient conditions may play a role, which needs to be studied further. However, OLA is susceptible to oxidation to form hydroxylamine [Eq. (b)]. It is possible that the oxidized amine groups coordinate to the atomically thin wire in the form of  $-C-N-O-Ti$ , passivating its surface in conjunction with OA and contributing to the surface N-doping of the atomically thin titania wire.



However, when the reaction temperature was increased to  $300^\circ C$ , the aminolysis rate was significantly increased so that titania wire growth could proceed much more rapidly, as established previously by Han and co-workers.<sup>[36]</sup> Now the amine could attack the carboxylate groups nucleophilically on the side-wall surface of the growing wire to form unstable titanium hydroxides, giving rise to thicker nanorods.<sup>[36]</sup>

In size-exclusion chromatographic analysis of the precursor solutions that were carried out to confirm our hypothesis, the precursor ( $\approx 10$  mg) was dispersed in hexane (2 mL, HPLC grade) and filtered through a syringe-driven filter ( $0.2 \mu m$ , Millex) before injection of the resulting solution into the HPLC column ( $20 \mu L$ ). Pure hexane was used as the mobile phase at a flow rate of  $3 mL \cdot min^{-1}$ . Because the optical absorption of the precursor is in the UV range (see Figure S2 in the Supporting Information), we chose the detector wavelength range of 230–240 nm. The chromatogram of pure OA (see Figure S3A in the Supporting Information) has two close signals at the elution time of 3.0–3.5 min. For the mixture of OA, titanium butoxide, and cyclohexane obtained by stirring in ambient conditions at room temperature for 1 h and then extraction with ethanol (a condition for forming the pure precursor for the 1.8 nm nanowires), additional broad signals arose in the chromatogram in the 4–10 min elution time range (see Figure S3B in the Support-

ing Information), perhaps due to the variously substituted Ti complexes. The precursor resulting from heating the mixture at  $150^\circ C$  in an autoclave for 25 h followed by extraction with ethanol gave rise to a relatively sharp, strong signals at approximately 4 min (broken line in Figure S3C in the Supporting Information). The shortening of the elution time and the sharpening of the signals indicate that after the solvothermal procedure, the precursor with a relatively well-defined size was produced, which was probably the Ti dimer complex described above. A trailing tail extending to approximately 6 min can be interpreted as indicating the existence of some smaller molecules, for example, dimer or monomer complexes with different extents of substitutions.

We also used NMR spectroscopy to study the titania wire growth mechanism. The samples were prepared by dispersion in deuteriochloroform ( $CDCl_3$ , 1 mL; TMS, 1% v/v) by using approximately 2 mg in 1 mL  $CDCl_3$  for the precursor and 2 mg in 2 mL  $CDCl_3$  for the atomically thin wires to obtain homogeneous solutions. For comparison, the  $^1H$ NMR spectrum of pure OA was recorded by dispersing OA ( $\approx 0.1$  mL) in  $CDCl_3$  (1 mL). All the  $^1H$  spectra were obtained with only a single scan, whereas  $^{13}C$  spectra were averaged over 2750 scans.

Figure 9 shows the  $^1H$  NMR spectra of pure OA (A), precursor (B), and atomically thin wires (C), together with simulated  $^1H$  NMR results (obtained by using ChemOffice 2004) on the right of the figure for some possible  $^1H$ -containing species in the system. Here we focus on several characteristic signals numbered 1–8 in Figure 9 for comparison. First, all three samples exhibit a chemical shift signal at approximately 5.4 ppm (1), which corresponds to the H atoms on the double bond of OA ( $-CH=CH-$ ). This again indicates that both the precursor and the atomically thin wires contain the OA chains. However, in both of them, the signal at approximately 11 ppm (2) associated with the H atom in the  $-COOH$  group disappears. This is consistent with our perception that the carboxylic groups of all the surface-bound OA chains have been bonded to Ti atoms of the atomically thin wires. Signals 3 and 4 relate to the H atom closest to the carboxylic group in OA. The obvious broadening of the signals for the precursor and atomically thin wires compared with that of the pure OA is due to the reduced degree of freedom arising from the anchoring of the carboxylic groups to the relatively bulky precursor and atomically thin wires. Signal 5 is essentially the same for all the samples because this signal results from the H atoms that are relatively far away from the anchoring site of Ti atoms. Some new signals such as 6 and 7 can be attributed to the existence of by-products, such as 1-butanol and butyl oleate. Finally, we tentatively assign the new signals at approximately 2.7 (8) and 2.0 ppm (9) in the NMR spectrum of the atomically thin wires to the H atoms attached to the C and N atoms in  $-CH_2-NH-O-Ti$ , respectively, both of which presumably originate from the OLA added to the reaction system in the post-treatment step as described above. No signal was detected at approximately 8 ppm, which would be characteristic of H in  $R'-CO-NH-R''$ . This supports our

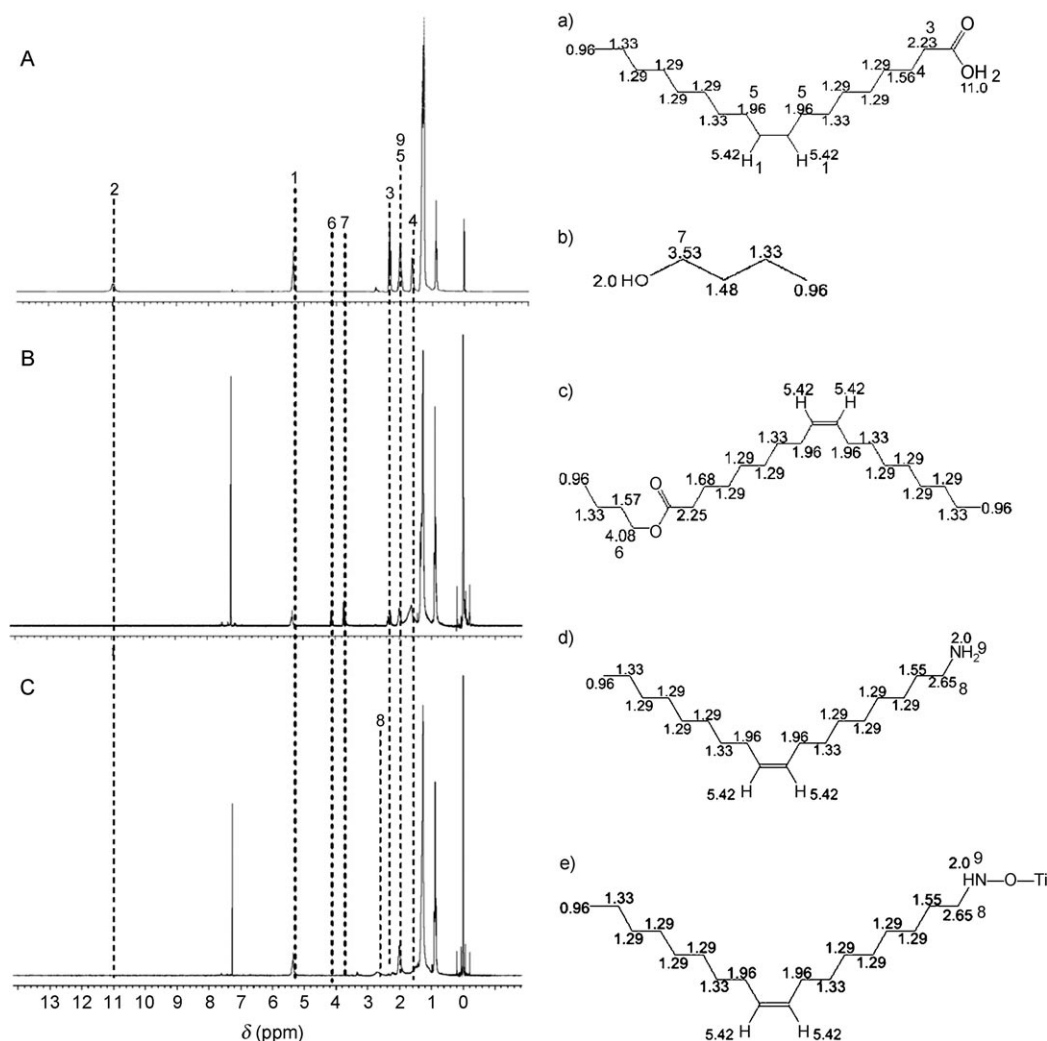


Figure 9. <sup>1</sup>H NMR spectra of A) pure OA, B) the precursor, and C) atomically thin wires. The calculated results for possible species in the reaction system are presented on the right for a) OA, b) butanol, c) butyl oleate, d) oleylamine, and e) a possible N–O–Ti structure.

belief that aminolysis is likely to be inconsequential during the formation of the precursor and the atomically thin wires.

The  $^{13}\text{C}$  NMR spectra of pure OA (A) and atomically thin wires (B) are shown in Figure S4 in the Supporting Information. First, in accordance with the  $^1\text{H}$  NMR result, the presence of the C=C double bond in the OA in the atomically thin wires is confirmed by signal 1. Second, the  $^{13}\text{C}$  atom in the carboxylic group (signal 2 in the OA spectrum) shows an approximately 174 ppm NMR shift to higher field for the atomically thin wires, in good agreement with the result estimated by using the ChemOffice 2004 software. Third, a new signal at approximately 46 ppm arises in the NMR spectrum of the atomically thin wires, which is fairly consistent with the C-N-O-Ti structure proposed above (see signal 3 in Figure S4B in the Supporting Information and the estimated result). This result is further support for our proposition that the N-doping in the atomically thin wires is in the form of C-N-O-Ti on their surfaces.

To address the question of why the  $\text{TiO}_2$  products are prone to grow in one dimension under our synthetic condi-

tions, we emphasize the importance of surface energy. Specifically, because the (001) planes of anatase titania have higher surface energy, the Ti–O–Ti network preferentially extends along the [001] direction during the growth of TiO<sub>2</sub> nanocrystals. We further believe that the facile N-doping also results from surface stabilization by the OLA molecules.

## Conclusion

We have described the synthesis of nearly monodisperse, ambient-condition stable, ultrathin anatase titania wires with sizes tunable between 5 and 0.4 nm by a nonhydrolytic two-step approach. Size control of the wires was achieved by formation of a precursor, its restricted esterification, and the attendant growth of the wires. Surface N-doping was shown to be significant for the atomically thin titania wires because of their extremely large specific surface area. In addition, the surface N-doping was found to stabilize the atomically

thin anatase titania wires further because the amine molecules work as both a dopant and a surfactant. Both the size reduction and the surface N-doping were demonstrated to have dramatic effects on the electronic, optical, and vibrational properties of the atomically thin wires. In particular, extreme size reduction of anatase wires has increased the electronic bandgap by at least 1 eV, and has radically shifted and broadened the phonon spectrum. The N-doping on the atomically thin anatase wire surfaces has also introduced bandgap states and has given atomically thin wires with the capability to absorb in the visible region of electromagnetic radiation. This opens up new avenues and will invigorate endeavors to tailor material properties, which in turn will aid the design of future devices at the nano-, molecular, and atomic scales. In addition, the nonhydrolytic two-step approach may be applied to the synthesis of ultrathin nanorods or nanowires and atomically thin wires of other oxide and chalcogenide materials.

## Experimental Section

**Materials and reagents:** Titanium butoxide (Alfa Aesar, 98%), OA (95%, International Laboratory USA), OLA (Aldrich, 70%), cyclohexane (Acros), and octadecene (Sigma-Aldrich, 90%) were used as received without further purification. Other chemicals were of analytical grade and were also used as received without further purification.

**Synthesis of atomically thin anatase titania wires:** Appropriate amounts of OA (3 mL) and cyclohexane (10 mL) were mixed, and  $\text{Ti}(\text{OBU})_4$  (0.5 mL) was slowly added dropwise to the mixed solution. The resulting solution was sealed in a Teflon-lined stainless autoclave, heated to 150°C and kept at that temperature for 25 h. A light-yellow, sticky, titanium complex precursor (viscous but transparent) was obtained, which was then extracted by precipitation with an excess of ethanol at RT.

The titanium complex precursor was redispersed in a mixture of ODE (5 mL), OA (0.6 mL), and OLA (0.8 mL). The solution was heated to and maintained at 180°C in a three-necked flask with stirring for 1 h under ambient conditions. The mixture appeared to be clear and light-yellow, and then turned darker yellow as the reaction proceeded, indicating the formation of N- $\text{TiO}_2$  products.

Product extraction was performed in air at room temperature. When an excess of ethanol was added to the reaction mixture, the atomically thin N- $\text{TiO}_2$  wire product was precipitated. The precipitate was further purified by centrifugation and washed twice with ethanol to remove residual surfactants. The final atomically thin N- $\text{TiO}_2$  wires protected by OA-coordination were easily re-dispersed in solvents such as chloroform or hexane without any sign of further growth or irreversible aggregation.

**Synthesis of  $\text{TiO}_2$  nanorods:**  $\text{TiO}_2$  nanorods were prepared in the same way as the atomically thin wires except that the solvothermally treated precursor was post-treated in the presence of ODE at 300°C for a specified period of time.

For comparison, two other methods were used to synthesize  $\text{TiO}_2$  nanorods. In a one-step variant of the above-method method, a mixture of  $\text{Ti}(\text{OBU})_4$  (0.1 mL), OA (3 mL), and cyclohexane (10 mL) was stirred at room temperature for 1 h, and then OLA (1 mL) was added dropwise. The resulting solution was sealed in a Teflon-lined stainless autoclave, heated to 150°C, and kept for 25 h. The light-yellow precipitate obtained was extracted and washed as described above. The second method involved hot injection. After preparation of the precursor in the same way as for the synthesis of the atomically thin wires followed by mixing of OA (3 mL) and cyclohexane (10 mL),  $\text{Ti}(\text{OBU})_4$  (0.5 mL) was slowly dropped into the mixture. The resulting solution was sealed in a Teflon-lined stainless autoclave, heated to 150°C, and kept at that temperature

for 25 h. The titanium complex precursor was extracted by precipitation with an excess of ethanol at room temperature, then re-dispersed in a mixture of ODE (5 mL) and OA (0.6 mL). The solution was heated to and maintained at 300°C in a three-necked flask with stirring for 30 min, followed by injection of OLA (0.8 mL). After reaction for 30 min, a grayish-white product was obtained by extraction with an excess of ethanol, centrifugation, and was washed twice with ethanol.

**Characterization:** The prepared products were characterized by TEM and HRTEM by using JEOL 2010 and JEOL 2010F microscopes with an accelerating voltage of 200 kV. Samples for TEM measurements were prepared by sonicating the precipitate products in hexane for 30 min and evaporating a drop of the suspension onto a carbon-coated, porous film supported on a copper grid. The XPS spectra were measured on a Perkin-Elmer model PHI 5600 XPS system with a resolution of 0.3–0.5 eV from a monochromated aluminium anode X-ray source with  $\text{Mo}_{\text{K}\alpha}$  radiation (1486.6 eV). The samples were prepared by dispersing the powder products on a carbon tape, which was attached to the sample holder. The binding energies of Ti2p, O1s, C1s, and N1s peaks from the samples were calibrated with respect to the C1s peak from the carbon tape at 285 eV. UV/Vis spectra were measured on a Milton-Roy Spectronic 3000 Array instrument. Photoluminescence spectra were measured by using a Perkin-Elmer luminescence spectrometer, Model LS-55. FTIR analysis was carried out by using pressed KBr disks in the 4000–400  $\text{cm}^{-1}$  region in a Perkin-Elmer spectrometer. Raman scattering spectroscopy at RT in a Renishaw RM 3000 micro-Raman system (spectral resolution  $<1 \text{ cm}^{-1}$ ), employed an  $\text{Ar}^+$  laser for excitation ( $\lambda=514 \text{ nm}$ , power  $\approx 25 \text{ mW}$ ). ESR measurements were undertaken at RT with a JEOL ES-IPRITS ESR spectrometer operating at X-band frequency ( $\approx 9.4 \text{ GHz}$ ). The white-light illumination was generated by a 150 W halogen light source (DCR III, Schott North America).

A Varian Mercury 300 MHz NMR spectrometer was used for NMR spectroscopy. For MS (MALDI-TOF), a MALDI Micro MX TM mass spectrometer (Waters Micromass) was employed. Size-exclusion chromatography was performed by using a Waters HPLC system 600-717–996 equipped with a gel permeation column (American Polymer Standards Corporation; porosity: linear 10  $\mu\text{m}$ ; serial no.: 7-7-92).

## Acknowledgements

This work was supported by the Research Grants Council of Hong Kong (GRF nos. 604206 and 604608).

- [1] B. J. Holliday, C. A. Mirkin, *Angew. Chem.* **2001**, *113*, 2076–2097; *Angew. Chem. Int. Ed.* **2001**, *40*, 2022–2043.
- [2] C. Sanchez, G. J. A. A. de Soler-Illia, F. Ribot, T. Lalot, C. R. Mayer, V. Cabuil, *Chem. Mater.* **2001**, *13*, 3061–3083.
- [3] Y. Mao, T.-J. Park, F. Zhang, H. Zhou, S. S. Wong, *Small* **2007**, *3*, 1122–1139.
- [4] A. P. Alivisatos, *Science* **1996**, *271*, 933–937.
- [5] C. B. Murray, D. J. Norris, M. G. Bawendi, *J. Am. Chem. Soc.* **1993**, *115*, 8706–8715.
- [6] X. Peng, L. Manna, W. Yang, J. Wickham, E. Scher, A. Kadavanich, A. P. Alivisatos, *Nature* **2000**, *404*, 59–61.
- [7] C. Burda, X. Chen, R. Narayanan, M. A. El-Sayed, *Chem. Rev.* **2005**, *105*, 1025–1102, and references therein.
- [8] J. Park, J. Joo, S. G. Kwon, Y. Jang, T. Hyeon, *Angew. Chem.* **2007**, *119*, 4714–4745; *Angew. Chem. Int. Ed.* **2007**, *46*, 4630–4660.
- [9] T. Yu, J. Joo, Y. Park II, T. Hyeon, *J. Am. Chem. Soc.* **2006**, *128*, 1786–1787.
- [10] Z. Huo, C. Tsung, W. Huang, X. Zhang, P. Yang, *Nano Lett.* **2008**, *8*, 2041–2044.
- [11] Z. Huo, C.-K. Tsung, W. Huang, M. Fardy, R. Yan, X. Zhang, Y. Li, P. Yang, *Nano Lett.* **2009**, *9*, 1260–1264.
- [12] M. R. Hoffmann, S. T. Martin, W. Choi, D. W. Bahnemann, *Chem. Rev.* **1995**, *95*, 69–96, and references therein.

- [13] X. Chen, S. S. Mao, *Chem. Rev.* **2007**, *107*, 2891–2959, and references therein.
- [14] B. O'Regan, M. Grätzel, *Nature* **1991**, *353*, 737–740.
- [15] A. Fujishima, K. Honda, *Nature* **1972**, *238*, 37–38.
- [16] O. K. Varghese, D. Gong, M. Paulose, K. G. Ong, C. A. Grimes, *Sens. Actuators B* **2003**, *93*, 338–344.
- [17] G. F. Ortiz, I. Hanzu, T. Djenizian, P. Lavela, J. L. Tirado, P. Kauth, *Chem. Mater.* **2009**, *21*, 63–67.
- [18] G. F. Ortiz, I. Hanzu, P. Knauth, P. Lavela, J. L. Tirado, T. Djenizian, *Electrochim. Acta* **2009**, *54*, 4262–4268.
- [19] R. Levinson, P. Berdahl, H. Akbari, *Sol. Energy Mater. Sol. Cells* **2005**, *89*, 319–349.
- [20] R. Asahi, T. Morikawa, T. Ohwaki, K. Aoki, Y. Taga, *Science* **2001**, *293*, 269–271.
- [21] S. Sato, *Science* **2002**, *295*, 626–627.
- [22] S. Sato, *Chem. Phys. Lett.* **1986**, *123*, 126–128.
- [23] C. Burda, Y. Lou, X. Chen, A. C. S. Samia, J. Stout, J. L. Gole, *Nano Lett.* **2003**, *3*, 1049–1051.
- [24] H. Irie, Y. Watanabe, K. Hashimoto, *J. Phys. Chem. B* **2003**, *107*, 5483–5486.
- [25] X. Chen, Y. Lou, Y. A. C. S. Samia, C. Burda, J. L. Gole, *Adv. Funct. Mater.* **2005**, *15*, 41–49.
- [26] S. M. Prokes, J. L. Gole, X. Chen, C. Burda, W. E. Carlos, *Adv. Funct. Mater.* **2005**, *15*, 161–167.
- [27] X. Qiu, Y. Zhao, C. Burda, *Adv. Mater.* **2007**, *19*, 3995–3999.
- [28] T. Ma, M. Akiyama, E. Abe, I. Imai, *Nano Lett.* **2005**, *5*, 2543–2547.
- [29] X. Chen, C. Burda, *J. Phys. Chem. A* **2004**, *108*, 15446–15449.
- [30] S. Livraghi, M. C. Paganini, E. Giamello, A. Selloni, C. D. Valentin, G. Pacchioni, *J. Am. Chem. Soc.* **2006**, *128*, 15666–15671.
- [31] X.-L. Li, Q. Peng, J.-X. Yi, X. Wang, Y. Li, *Chem. Eur. J.* **2006**, *12*, 2383–2391.
- [32] X. Jiang, T. Herricks, Y. Xia, *Adv. Mater.* **2003**, *15*, 1205–1209.
- [33] M. Kobayashi, V. V. Petrykin, M. Kakihana, *Chem. Mater.* **2007**, *19*, 5373–5376.
- [34] Y.-W. Jun, M. F. Casula, J.-H. Sim, S. Y. Kim, J. Cheon, A. P. Alivisatos, *J. Am. Chem. Soc.* **2003**, *125*, 15981–15985.
- [35] P. D. Cozzoli, A. Kornowski, H. Weller, *J. Am. Chem. Soc.* **2003**, *125*, 14539–14548.
- [36] Z. Zhang, X. Zhong, S. Liu, D. Li, M. Han, *Angew. Chem.* **2005**, *117*, 3532–3536; *Angew. Chem. Int. Ed.* **2005**, *44*, 3466–3470.
- [37] Y. C. Hong, J. H. Kim, C. U. Bang, H. S. Uhm, *Phys. Plasmas* **2005**, *12*, 114501.
- [38] Y.-W. Jun, J.-H. Lee, J.-S. Choi, J. Cheon, *J. Phys. Chem. B* **2005**, *109*, 14795–14806.
- [39] R. Buonsanti, V. Grillo, E. Carlino, C. Giannini, T. Kipp, R. Cingolani, P. D. Cozzoli, *J. Am. Chem. Soc.* **2008**, *130*, 11223–11233.
- [40] B. Xiang, Y. Zhang, Z. Wang, X. H. Luo, Y. W. Zhu, H. Z. Zhang, D. P. Yu, *J. Phys. D: Appl. Phys.* **2005**, *38*, 1152–1155.
- [41] Y. Lin, G. S. Wu, X. Y. Yuan, T. Xie, L. D. Zhang, *J. Phys. Condens. Matter* **2003**, *15*, 2917–2922.
- [42] C. Liu, S. Yang, *ACS Nano* **2009**, *3*, 1025–1031.
- [43] R. Si, Y.-W. Zhang, H.-P. Zhou, L.-D. Sun, C.-H. Yan, *Chem. Mater.* **2007**, *19*, 18–27.
- [44] P. D. Cozzoli, T. Pellegrino, L. Manna, *Chem. Soc. Rev.* **2006**, *35*, 1195–1208.
- [45] J. F. Moulder, W. F. Stickle, P. E. Sobol, K. D. Bomben, *Handbook of X-Ray Photoelectron Spectroscopy*, Perkin-Elmer, Wiesbaden, **1992**, pp. 43–45.
- [46] Q. Guo, Y. Xie, X. Wang, S. Zhang, T. Hou, S. Lv, *Chem. Commun.* **2004**, 26–27.
- [47] A. P. Dementjev, A. de Graaf, M. C. M. van de Sanden, K. I. Maslakov, A. V. Naumkin, A. A. Serov, *Diamond Relat. Mater.* **2000**, *9*, 1904–1907.
- [48] C. Burda, J. Gole, *J. Phys. Chem. B* **2006**, *110*, 7081–7082.
- [49] S. Livraghi, A. Votta, M. C. Paganini, E. Giamello, *Chem. Commun.* **2005**, 498–500.
- [50] S. Hashimoto, A. Murata, T. Sakurada, A. Tanaka, *J. Surf. Anal.* **2002**, *9*, 459–462.
- [51] T. Ohsaka, F. Izumi, Y. Fujiki, *J. Raman Spectrosc.* **1978**, *7*, 321–324.
- [52] V. Swamy, A. Kuznetsov, L. S. Dubrovinsky, R. A. Caruso, D. G. Shchukin, B. C. Muddle, *Phys. Rev. B* **2005**, *71*, 184302.
- [53] H. C. Choi, Y. M. Jung, S. B. Kim, *Vib. Spectrosc.* **2005**, *37*, 33–38.
- [54] S. Kelly, F. H. Pollak, M. Tomkiewicz, *J. Phys. Chem. B* **1997**, *101*, 2730–2734.
- [55] C. J. Doss, R. Zallen, *Phys. Rev. B* **1993**, *48*, 15626–15637.
- [56] M. J. Pelletier, *Analytical Applications of Raman spectroscopy*, Blackwell-Science, Malden, **1999**.
- [57] D. Bersani, P. P. Lottici, *Appl. Phys. Lett.* **1998**, *72*, 73–75.
- [58] J. Zi, K. M. Zhang, X. D. Xie, *Phys. Rev. B* **1997**, *55*, 9263–9265.
- [59] A. Williams, *Acc. Chem. Res.* **1999**, *32*, 387–392.
- [60] J. C. Parker, R. W. Siegel, *Appl. Phys. Lett.* **1990**, *57*, 943–945.
- [61] J. C. Parker, R. W. Siegel, *J. Mater. Res.* **1990**, *5*, 1246–1252.
- [62] W. Ma, Z. Lu, M. Zhang, *Appl. Phys. A* **1998**, *66*, 621–627.
- [63] Y. Liu, R. O. Claus, *J. Am. Chem. Soc.* **1997**, *119*, 5273–5274.
- [64] D. Pan, N. Zhao, Q. Wang, S. Jiang, X. Ji, L. An, *Adv. Mater.* **2005**, *17*, 1991–1995.
- [65] R. Beranek, H. Kisch, *Photochem. Photobiol. Sci.* **2008**, *7*, 40–48.
- [66] N. Serpone, *J. Phys. Chem. B* **2006**, *110*, 24287–24293.
- [67] F. Dong, W. Zhao, Z. Wu, S. Guo, *J. Hazard. Mater.* **2009**, *162*, 763–770.
- [68] J. Zhang, Y. Hu, M. Matsuoka, H. Yamashita, M. Minagawa, H. Hidaka, M. Anpo, *J. Phys. Chem. B* **2001**, *105*, 8395–8398.
- [69] Y. Cong, J. Zhang, F. Chen, M. Anpo, *J. Phys. Chem. C* **2007**, *111*, 6976–6982.
- [70] J. Zhou, M. Takeuchi, A. K. Ray, M. Anpo, X. Zhao, *J. Colloid Interface Sci.* **2007**, *311*, 497–501.
- [71] Y. Nakaoka, Y. Nosaka, *J. Photochem. Photobiol. A* **1997**, *110*, 299–305.
- [72] J. M. Coronado, A. J. Maira, J. C. Conesa, K. L. Yeung, V. Augugliaro, J. Soria, *Langmuir* **2001**, *17*, 5368–5374.
- [73] R. F. Howe, M. Gratzel, *J. Phys. Chem.* **1987**, *91*, 3906–3909.
- [74] O. I. Micic, Y. Zhang, K. R. Cromack, A. D. Trifunac, M. C. Thurnauer, *J. Phys. Chem.* **1993**, *97*, 7277–7283.
- [75] A. R. González-Elipe, J. Soria, G. Munuera, *Chem. Phys. Lett.* **1978**, *57*, 265–268.
- [76] S.-K. Joung, T. Amemiya, M. Murabayashi, K. Itoh, *Chem. Eur. J.* **2006**, *12*, 5526–5534.
- [77] T. Rajh, A. E. Ostafin, O. I. Micic, D. M. Tiede, M. C. Thurnauer, *J. Phys. Chem.* **1996**, *100*, 4538–4545.

Received: September 14, 2009  
Published online: March 5, 2010